Mitsuuchi Tashima, M.; Soriano Martinez, L.; Borrachero Rosado, MV.; Monzó Balbuena, JM.; Cheeseman, CR.; Paya Bernabeu, JJ. (2012). Alkali activation of vitreous calcium aluminosilicate derived from glass fiber waste. Journal of Sustainable Cement-Based Materials. 1(3):83-93. doi:10.1080/21650373.2012.742610.

ALKALI-ACTIVATION OF VITREOUS CALCIUM ALUMINOSILICATE DERIVED FROM GLASS FIBRE WASTE

M.M. Tashima[1], L. Soriano[1], M.V. Borrachero[1], J. Monzó[1], C.R. Cheeseman[2*], J. Payá[1]

[1]Instituto de Ciencia y Tecnología del Hormigón, Universitat Politècnica de València, Camino de Vera s/n, Edificio 4G, 46022 Valencia, Spain

[2]Department of Civil and Environmental Engineering, Imperial College London, London SW7 2AZ, UK

*Corresponding author: c.cheeseman@imperial.ac.uk

E-mail addresses: maumitta@hotmail.com, lousomar@upvnet.upv.es, vborrachero@cst.upv.es, jmmonzo@cst.upv.es, jjpaya@cst.upv.es

ABSTRACT

The properties and microstructure of alkali-activated vitreous calcium aluminosilicate (VCAS) are presented in this paper. VCAS is manufactured from a by-product of the glass fibre industry and has been activated using NaOH and KOH solutions. The microstructure and mechanical properties of alkali-activated VCAS pastes and mortars are reported. The results show that depending on the type and concentration of hydroxide solution used, mortar samples with compressive strengths up to 77 MPa can be formed after curing for 3 days at 65ºC. The research demonstrates the potential of VCAS to produce alkali-activated cements and the importance of alkali type and concentration in optimising properties and microstructure.

***Keywords*:** Alkali-activated binder, Vitreous calcium aluminosilicate, VCAS, Alkali concentration, Microstructure

1. INTRODUCTION

There is significant interest world-wide in the development of more sustainable cementitious materials due to the environmental issues associated with the manufacture of Portland cement. In 2008 approximately 2,600 million tonnes of Portland cement were produced and this is expected to increase by ~225% by 2050 (Mahasenan et al., 2003; Schneider et al., 2011). It is estimated that Portland cement production is currently responsible for 5-8% of global CO_2 emissions due to the high temperatures required for Portland cement production and the use of limestone ($CaCO_3$) as a major raw material.

The use of supplementary cementitious materials (SCM) in blended cements, mortars and the production of Portland cement is increasing. The CO_2 resulting from partial replacement of Portland cement by mineral additions is reported to be reduced from approximately 886 kg for pure clinker to ~660 kg of CO_2 per tonne of cement (WBCSD, 2009), giving a typical reduction of more than 200 Kg per tonne of Portland cement. However, research efforts are also focusing on the production of alternative cementitious materials that have lower CO_2 emissions, and alkali-activated (AA) cements have particular potential. Reduction in CO_2 emissions by up to 80% has been achieved and the performance of AA cements can be improved in some aspects in comparison to Portland cement (Shi et al., 2011).

Alkali activation results in networks of SiO_4 and AlO_4 tetrahedra linked by sharing oxygen atoms. Positive ions such as Na^+, K^+, Mg^{2+} or Ca^{2+} must be present in the framework cavities to balance the charge deficiency of Al^{3+} compared to Si^{4+}. This forms a three dimensional network of Si^{4+} and Al^{3+} in 4-fold coordination with oxygen (Duxson et al., 2007; Fernández-Jiménez et al., 2005).

In this paper the use of vitreous calcium aluminosilicate (VCAS) is reported as this a potential material for the production of alkali-activated cements. VCAS is a pozzolan derived from melting, quenching and grinding waste glass fibre. It has previously been used as an admixture in the production of Portland cement mortars and concretes (Hossain and Shirazi, 2008; Neithalath et al., 2009). The effect of curing time on the microstructure and mechanical

properties of VCAS activated using 10 mol.kg^{-1} NaOH solution has recently been reported (Tashima et al., 2012) and this concluded that the optimum curing conditions were 65 ºC at relative high humidity (RH~95%).

The aim of this work was to investigate the effect of the concentration of NaOH and KOH activating solution on the microstructure and mechanical strength of alkali-activated VCAS pastes and mortars.

2. EXPERIMENTAL

2.1 Materials

VCAS was obtained from Vitro Minerals USA, as a white powder, produced by melting, quenching and grinding of waste glass fibre (Hemmings et al., 2004). The chemical composition of VCAS, determined by X-ray fluorescence (XRF) is given in Table 1. Previous work has shown that VCAS can exhibit significant pozzolanic activity (Neithalath et al., 2009).

Figure 1 shows a scanning electron micrograph image of VCAS and indicates irregular, dense and often sharp particles with a wide range of particle sizes. The particle size distribution was determined by laser diffraction and this indicated a mean particle diameter of approximately 12 μm, with 90% of particles (by volume) less than 26 μm.

Sodium hydroxide (NaOH, 95% purity) and potassium hydroxide (KOH, 85% purity) pellets were supplied by Panreac SA. These were used to prepare alkali-activating solutions with different concentrations. Siliceous sand with a specific gravity of 2.68 g.cm^{-3} and fineness modulus of 4.1 (UNE-EN 196-1) was used to prepare mortar samples.

2.2 Tests performed on alkali-activated samples

Microstructural characterization of alkali-activated VCAS has used a range of techniques. X-ray diffraction (XRD, Philips PW1710 with Cu Kα radiation in 2θ range 5-55º) was used to characterise the crystalline and semi-crystalline phases in paste samples. Scanning electron microscopy (SEM, JEOL JSM-6300) was used to examine fracture

surfaces. FTIR (Mattson Genesis II spectrometer) of alkali-activated pastes used the KBr pellets technique (1:100) to prepare samples which were scanned between 4000 cm^{-1} and 400 cm^{-1}. Thermogravimetric analysis (TGA, 850 Mettler Toledo thermo-balance) used 100 μL aluminium crucibles and a nitrogen atmosphere. Samples were heated from 35 to 600ºC at 10ºC.min^{-1} to give total weight loss (%) data associated with the dehydration/dehydroxilation of alkali activated VCAS.

Strength tests used a universal test machine following the procedures described in UNE-EN 196-1. The compressive strength data presented is the average of six specimens. Mercury intrusion porosimetry (MIP, Micromeritics Instrument Corporation) was used to evaluate the pore size distribution in alkali-activated VCAS mortars. The intrusion pressure applied was between 14 kPa and 227.4 MPa, and this is equivalent to pores with diameters ranging from 91.26 μm to 5.5 nm.

2.3 Mix composition and sample preparation

Activating solutions were prepared by dissolving alkali hydroxide pellets in the required amount of water. The concentrations of both the Na^+ and the K^+ ranged from 2.5 to 12.5 mol.kg^{-1}. Table 2 summarizes the activating solutions used. The paste and mortar samples prepared using these solutions have been given the notation S*A*C, where S is the type of sample, paste (p) or mortar (m), A is the type of alkaline solution (NaOH or KOH) and *C* is the concentration of the alkaline solution (mol.kg^{-1}).

The alkali-activating solutions were prepared at least 30 minutes prior to use to allow the solutions to cool to room temperature. Alkali-activated paste samples were produced by mixing VCAS powder with the required amount of alkaline activating solution for 3 minutes. Paste samples were then cast and stored in 95% RH at 65ºC.

Alkali-activated VCAS mortar samples were prepared by mixing VCAS with activating solution for 4 minutes. Siliceous sand was then added to give a sand/VCAS mass ratio of 3, before being mixed for a further 3 minutes. The fresh mortars were cast in prismatic moulds (4x4x16 cm^3) and vibrated for 3 minutes to remove any air voids. The moulds were then sealed with plastic film to avoid atmospheric carbonation and stored in a thermal bath at

65ºC for 4 hours. Samples were then de-moulded and stored under the same curing conditions as the paste samples.

3. RESULTS AND DISCUSSION

3.1 X-ray diffraction studies

3.1.1 NaOH pastes

Figure 2 shows the XRD patterns of alkali-activated VCAS pastes activated with different concentrations of NaOH. Data for the as-received VCAS sample is also shown for comparison. This indicates that the as-received VCAS sample is amorphous, as indicated by the high background count in the range 17-32º. There is also evidence of quartz (SiO_2, PDF-card 331161) in the VCAS.

The formation of semi-crystalline to crystalline phases in the gel formed can be observed in pastes with increasing Na^+ concentration. The zeolites Na-P1 ($Na_6Al_{16}Si_{10}O_{32}.12H_2O$, PDF-card 390219) and sodalite ($1.8Na_2O.Al_2O_3.1.68SiO_2.1.8H_2O$, PDF-card 311271) was also identified. The presence of crystalline or semi-crystalline phases during the formation of alkali activated materials from selected mineral admixtures has previously been reported (Provis et al. 2005; Barbosa et al. 2000; Criado et al. 2007). Calcium carbonate (calcite, $CaCO_3$, PDF-card 050586) and sodium carbonate (natrite, Na_2CO_3, PDF-card 370451) were also detected and these phases are probably formed in alkali activated pastes due to carbonation or the presence of impurities in the sample (Rodríguez et al., 2012). CSH was also formed in the mixtures (Tobermorite 11Å, $Ca_5(OH)_2Si_6O_{16}.4H_2O$, PDF-card 191369) due to the high calcium content in VCAS.

3.1.2 KOH pastes

Figure 3 shows XRD data for KOH alkali activated pastes. The formation of crystalline phases during gel formation was not detected by XRD and these results are similar to those of Fernández-Jiménez et al. (2006) who found that alkali activated systems based on

fly ash activated by KOH had increased amorphous content compared to equivalent systems activated using NaOH.

The amorphous microstructure of pastes activated with KOH is indicated by the high background in the 20-35º 2 θ range, as shown in Figure 3. This is displaced to higher 2θ angles when VCAS is activated under more alkaline concentrations. Provis et al. (2005) suggested this displacement in the baseline deviation is a characteristic of gel formation.

3.2 Fourier transform infrared (FTIR) spectroscopy studies

3.2.1 NaOH pastes

Figure 4 shows the FTIR spectra for the NaOH activated VCAS pastes. This indicates that significant changes occur at the nano-scale in alkali-activated VCAS pastes. The band corresponding to the asymmetric stretching vibration of Si-O-Si groups shifts from 1010 cm^{-1} to lower values (995-980 cm^{-1}) for VCAS activated with NaOH solutions. This shift is more pronounced with higher alkaline concentrations. In addition, the shoulder observed at 1100-1200 cm^{-1} in the FTIR spectrum of unreacted VCAS was reduced in intensity for pastes with high alkaline concentration. This behaviour indicates the formation of a new characteristic nanostructure associated with an amorphous gel in the alkali-activated system (Rees et al. 2007).

The second characteristic band for these systems is the peak centred around 460cm^{-1}. According to the literature (Lee and van Deventer, 2003; García-Lodeiro et al., 2008), this peak is characteristic of internal deformation vibrations of Si-O-Si and Si-O-Al bonds. The displacements of this peak to lower values, between 470 cm^{-1} to 455 cm^{-1}, can also be attributed to gel formation.

3.2.2 KOH pastes

Figure 5 shows the FTIR spectra for VCAS pastes activated with different concentrations of KOH. The displacement of the characteristic bands is similar to those obtained for VCAS pastes activated with NaOH solutions. In this case the range of the shift is

from 1003-995 cm^{-1}. All the characteristic bands of aluminosilicate materials are shifted to lower frequencies. The presence of the band centred at 1450 cm^{-1} is associated with the asymmetric stretching vibration of O-C-O groups resulting from carbonation.

3.3 Thermogravimetric analysis (TGA) studies

3.3.1 NaOH pastes

Thermogravimetric analysis data in Figure 6 and Table 3 shows the total weight loss is in the temperature range between 35 and 600ºC for alkali-activated VCAS pastes. In general, when increasing NaOH concentration, higher total weight loss of paste samples occurred. For NaOH concentrations greater than 10 $mol.kg^{-1}$ a reduction in the total weight loss is observed, as excess alkalis does not increase the amount of OH^- and H_2O groups bound to the gel formed (Barbosa, 1999). For alkali concentrations below 10 $mol.kg^{-1}$ the amount of OH^- and H_2O bound groups is reduced due to the lower dissolving capacity of the activating solution.

Figure 6 shows the TG and DTG curves for selected pastes where the most significant weight loss of the AA-VCAS pastes occurs between 100 and 200ºC. This is associated with physically bound and zeolitic water present in the products formed (Bernal et al. 2011).

3.3.2 KOH pastes

The total weight loss of AA-VCAS activated with KOH solutions is shown in Figure 6 and Table 3. The increase in the KOH concentration increases the total weight loss of pastes. The results suggest that NaOH has a more pronounced ability than KOH solutions to form gel, although K^+ is also reported to promote gel formation (Duxson et al., 2007). Alkaline activation of VCAS is enhanced by the Na^+ cation because VCAS particles are very dense and compact and therefore dissolution in the alkaline environment is the limiting process.

3.4 Scanning Electron microscopy (SEM) studies

3.4.1 NaOH pastes

Figure 7 shows micrographs of NaOH activated VCAS pastes using different concentrations of NaOH. The pNa5.0 paste shown in Figure 7a has a porous microstructure with a significant amount of partially and/or unreacted VCAS particles. The pNa10.0 paste shown in Figure 7b has a dense-compact and amorphous microstructure. However, some particles of partially reacted VCAS are also present. The alkali-activated VCAS system is composed of unreacted VCAS particles bound into an alkali-activated binder phase, and this forms a similar microstructure to a particle reinforced composite (Boccaccini et al., 1997). Similar microstructural features have been observed in other alkali-activated glass systems (Kourti et al., 2010).

The amorphous gel formed was characterized by EDX and identified as (N,C)ASH, a sodium/calcium aluminosilicate hydrate. It was not possible to identify the presence of CSH gel in this system, as would be formed in alkali-activated slags.

3.4.2 KOH pastes

KOH activated VCAS pastes have a similar microstructures to those obtained using NaOH solutions, as shown in Figure 8. Pastes activated with 5.0 $mol.kg^{-1}$ (pK5.0) have a porous microstructure, whereas for the 10 $mol.kg^{-1}$ activated system (pK10.0), a dense, compact and amorphous microstructure is formed.

The main difference between the microstructure obtained using NaOH and KOH solutions is that using pNa10.0 NaOH produces partially reacted VCAS particles that are surrounded by a defined layer of reaction products with lower Na content than those found in the matrix. For the pK10.0, the VCAS particles are surrounded by the matrix but there is no evidence of a K concentration gradient. This suggests that the degree of reaction is higher for the NaOH activating solution and products of different composition can be obtained when the

NaOH concentration decreases with time. This is in agreement with the high total weight loss (%) observed in TGA studies of NaOH activated VCAS pastes.

3.5 Compressive strength of alkali activated VCAS mortars

Compressive strengths of mortars prepared using different concentrations of NaOH and KOH activating solutions are given in Table 4. The strengths vary from 16 to 70 MPa, with higher compressive strengths obtained for NaOH compared to KOH based systems. Dissolution of VCAS is limited in KOH and this reduces mechanical strength. This is particularly noticeable for low to medium alkaline activator concentrations. For example, the 10 $mol.kg^{-1}$ prepared mortar sample (mNa10.0) had compressive strengths of 77 MPa for NaOH solution and 70MPa for KOH solution (mK10.0). It was also observed that for alkali concentrations greater than 10 $mol.kg^{-1}$ the compressive strength of the AA-VCAS reduced, in agreement with previous studies (Lampris et al., 2009; Wu and Sun, 2007; Kourti et al., 2010).

3.6 Mercury Intrusion Porosimetry (MIP) studies

The pore size distribution data obtained by MIP is shown in Figure 9 for alkali activated VCAS mortars prepared using 10 $mol.kg^{-1}$ of NaOH and KOH. For the same alkali-concentration (10 $mol.kg^{-1}$), NaOH solution yielded lower total porosity at 6.23% compared to 8.30% for the KOH solution. This suggests that NaOH solution promotes greater dissolution of VCAS and consequently a higher degree of reaction, resulting in binders with lower total porosity and higher compressive strength. KOH activated mortar had 24% of the total porosity below 10 nm pore size diameter, whereas the corresponding data for NaOH activated mortars yielded 8%. Despite the higher total porosity for the K system, the pore size diameters are smaller for KOH than those in NaOH activated VCAS.

4. CONCLUSIONS

Alkali-activation of vitreous calcium aluminosilicate (VCAS) using NaOH and KOH is reported, and this shows that the type of cation and concentration of the activating solution have a key role in the determining changes to the VCAS and the microstructural characteristics and physical properties of the paste and mortar samples formed. VCAS mortars have compressive strength in the range of 20-77 MPa when cured at 65ºC for 3 days. Microstructural studies show that an amorphous, dense, compact microstructure is produced using high alkali-concentration activators. NaOH and KOH concentration of 10 $mol.kg^{-1}$ resulted in the lowest total porosities and these correspond to alkali activated VCAS with good mechanical properties.

ACKNOWLEDGEMENTS

We would like to thank the Ministerio de Ciencia e Innovación (MICINN) of the Spanish Government (BIA2011-26947) and also FEDER for funding. We would also like to thank Vitrominerals for supplying the VCAS samples used in these experiments.

REFERENCES

Barbosa, V.F.F. (1999). "Sintese e caracterização de polissialatos." PhD thesis. In portuguese.

Bernal, S.A., Rodríguez, E.D., Mejía de Gutiérrez, R., Gordillo, M., Provis, J.L. 2011. "Mechanical and thermal characterization of geopolymers based on silicate-activated metakaolin/slag blends." J Mater Sci 46(16), 5477-5486.

Boccaccini, A.R., Bücker, M., Bossert, J., Marszalek, K. (1997). "Glass matrix composites from coal fly ash and waste glass." Waste Manage 17, 39-45.

Criado, M., Fernández-Jiménez, A., de la Torre, A.G., Aranda, M.A.G., Palomo, A. (2007). "An XRD study of the effect of the SiO_2/Na_2O ratio on the alkali activation of fly ash." Cem Concr Res 37(5), 671-679.

282 Duxson, P.; Fernández-Jiménez, A.; Provis, J; Lukey, G.; Palomo, A.; van Deventer, J.
283 (2007). “Geopolymer technology: the current state of the art.” J Mater Sci 42(9), 2917-
284 2933.
285 Fernández-Jiménez, A.; Palomo, A.; Criado, M. (2005). “Microstructure development of
286 alkali-activated fly ash cement: a descriptive model.” Cem Concr Res 35(6), 1204-1209.
287 Fernández-Jiménez, A., Palomo, A., Criado, M. (2006). “Activación alcalina de cenizas
288 volantes. Estudio comparativo entre activadores sódicos y potásicos.” Mater Constr
289 56(281), 51-65.
290 García-Lodeiro, I., Fernández-Jiménez, A., Blanco, M., Palomo, A. (2008). “FTIR study of
291 the sol–gel synthesis of cementitious gels: C–S–H and N–A–S–H.” J sol-gel Sci technol
292 45(1), 63-72.
293 Hemmings, R.T.; Nelson, R.D.; Graves, P.L.; Cornelius, B.J. (2004) “White pozzolan
294 composition and blended cements containing same.” PATENT US6776838.
295 Hossain, A., Shirazi, S.A. (2008). “Properties of concrete containing vitreous calcium
296 aluminosilicate pozzolan.” J Transp Res board, 32-38.
297 Kourtis, I., Amurtha Rani, D., Boccaccini, A.R., Cheeseman, C.R. (2010). “Production of
298 geopolymers using glass produced from DC plasma treatment of air pollution control
299 (APC) residues.” J Hazard Mater 176, 704-709.
300 Kourtis, I., Amurtha Rani, D., Boccaccini, A.R., Cheeseman, C.R. (2011). “Geopolymer
301 from DC plasma-treated air pollution control residues, metakaolin, and granulated blast
302 furnace slag.” J Mater Civ Eng 23(6), 735-740.
303 Lampris, C., Lupo, R., Cheeseman, C.R. (2009). “Geopolymerization of silt generated from
304 construction and demolition waste washing plants.” Waste Manage 29, 368-373.
305 Lee, W.K.W., van Deventer, J.S.J. (2003). “Use of infrared spectroscopy to study
306 geopolymerization of heterogeneous amorphous aluminosilicates.” Langmuir 19(21),
307 8726-8734.
308 Mahasenan, N.; Smith, S.; Humphreys, K. (2003). “The cement industry and global climate
309 change: current and potential future cement industry CO_2 emissions.” Greenhouse Gas

310 Control Technologies - 6th International Conference. Oxford: Pergamon, 2003. p. 995-
311 1000.
312 Neithalath, N., Persun, J., Hossain, A. (2009). “Hydration in high-performance cementitious
313 systems containing vitreous calcium aluminosilicate or silica fume.” Cem. Concr. Res.,
314 39(6), 473-481.
315 Provis, J., Lukey, G.C., van Deventer, J.S.J. (2005). “Do geopolymers actually contain
316 nanocrystalline zeolites? A re-examination of existing results.” Chem Mat 17(12), 3075-
317 3085.
318 Rees, C.A., Provis, J.L., Lukey, G.C., van Deventer, J.S.J. (2007). "In situ ATR-FTIR study
319 of the early stages of fly ash geopolymer gel formation." Langmuir 23, 9076-9082.
320 Rodríguez, E.D., Bernal, S.A., Provis, J.L., Payá, J., Monzó, J., Borrachero, M.V. (2012).
321 “Effect of nanosilica-based activators on the performance of an alkali-activated fly ash
322 binder.” Cem Concr Comp, in press.
323 Schneider, M., Romer, M., Tschudin, M., Bolio, H. (2011). “Sustainable cement production-
324 present and future.” Cem Concr Res 41(7), 642-650.
325 Shi, C., Fernández-Jiménez, A., Palomo, A. (2011). “New cements for the 21st century: The
326 pursuit of an alternative to Portland cement.” Cem Concr Res 41(7), 750-763.
327 Tashima, M.M.; Soriano, L.; Borrachero, M.V.; Monzó, J.; Payá, J. (2012) “Effect of curing
328 time on the microstructure and mechanical strength development of alkali activated binders
329 based on Vitreous Calcium Aluminosilicate (VCAS)”. Bull Mater Sci: accepted for
330 publication.
331 Wu, H.C., Sun, P. (2007). “New building materials from fly ash-based lightweight inorganic
332 polymer.” Constr Build Mater 21, 211-217.
333 WBCSD – World Business Council for Sustainable Development. (2009). “Cement industry
334 energy and CO_2 performance – Getting numbers right”.
335
336
337
338

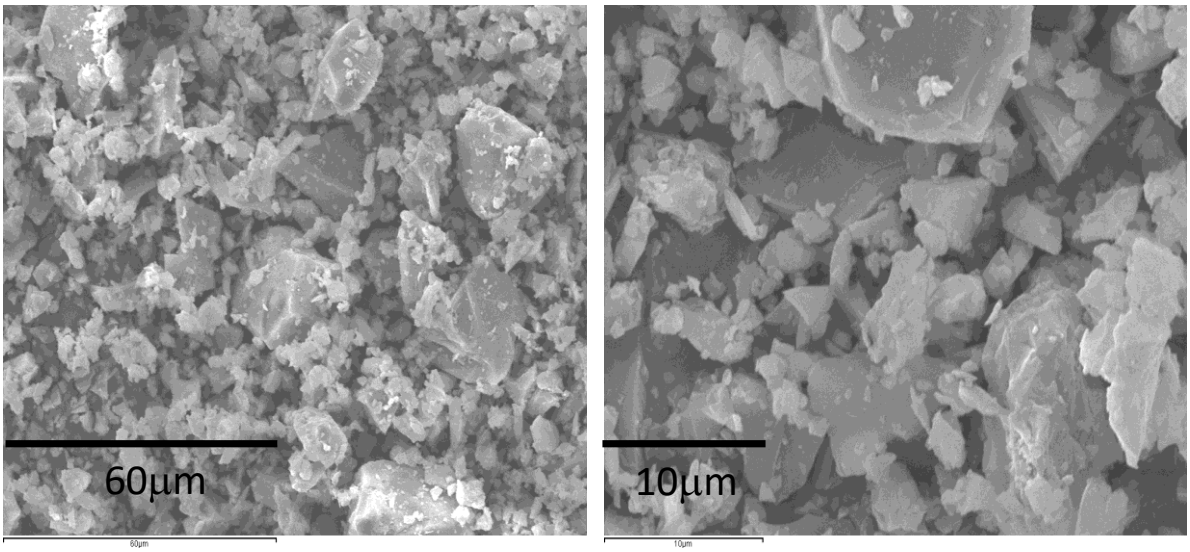

Figure 1. SEM images of VCAS particles.

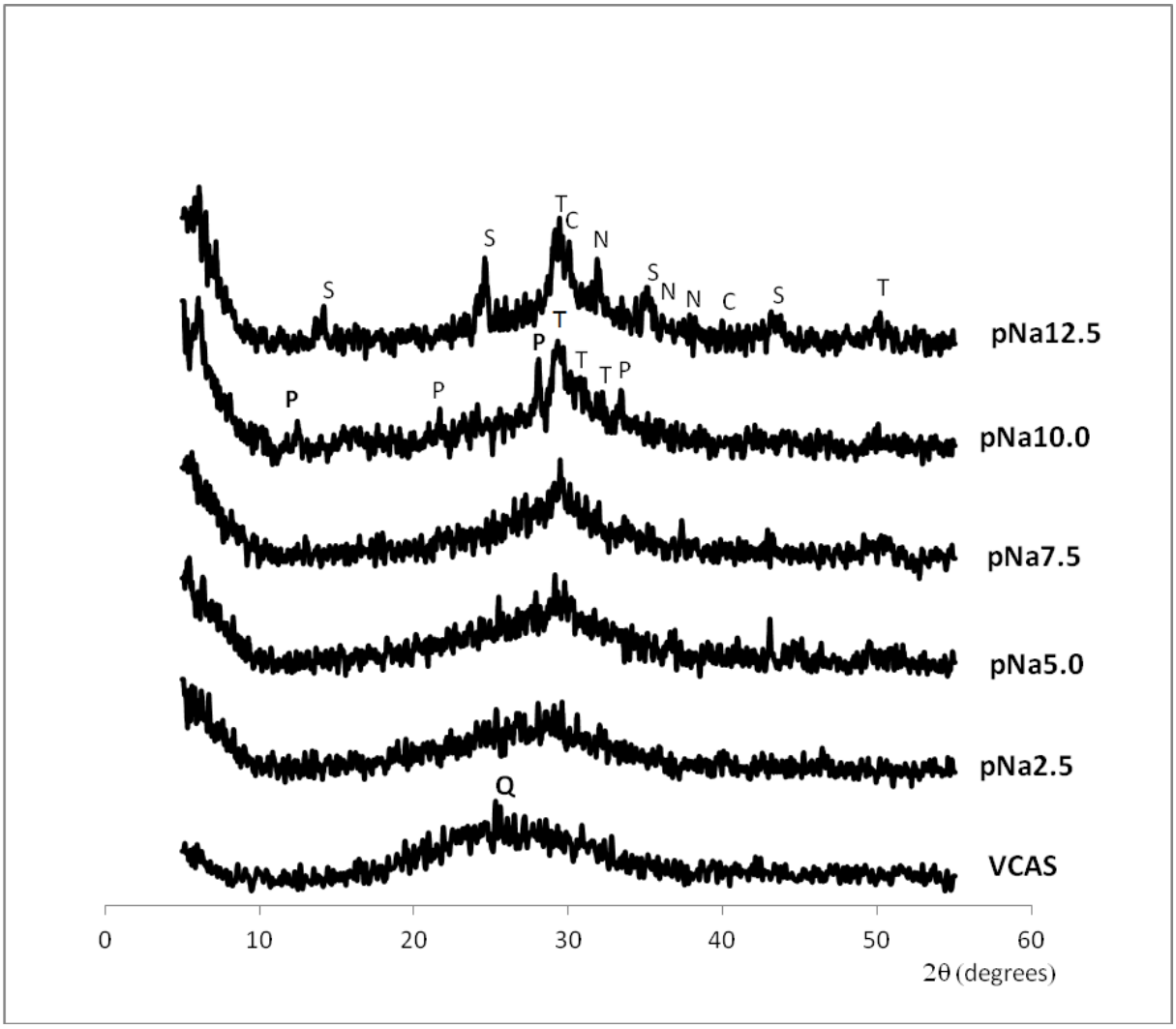

355

356 Figure 2. XRD data of alkali-activated VCAS activated using different concentrations of

357 NaOH. (Q: Quartz; P: Na-P1 zeolite; S: Sodalite; C: Calcite; N: Natrite; T: Tobermorite)

358

359

360

361

362

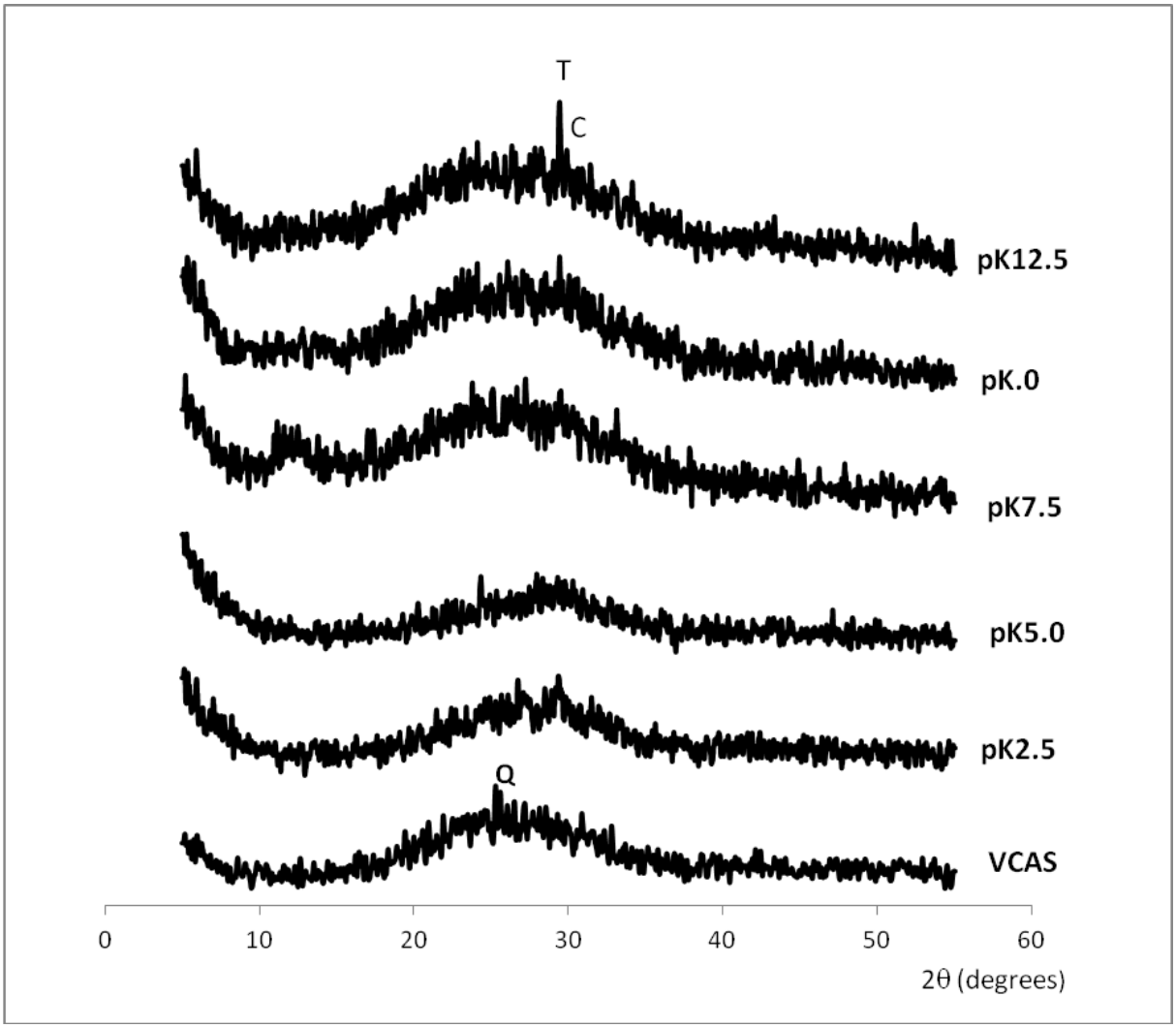

Figure 3. XRD data of alkali activated VCAS activated with different concentration of KOH. (Q: Quartz; C: Calcite; T: Tobermorite)

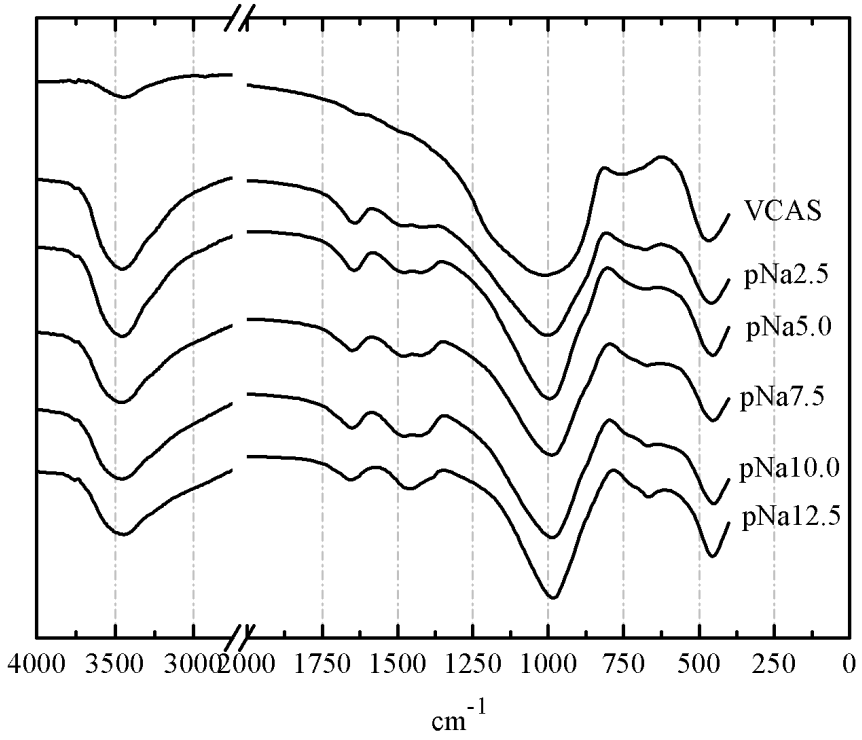

Figure 4. FTIR spectra for VCAS sample and AA-VCAS pastes activated with NaOH solutions.

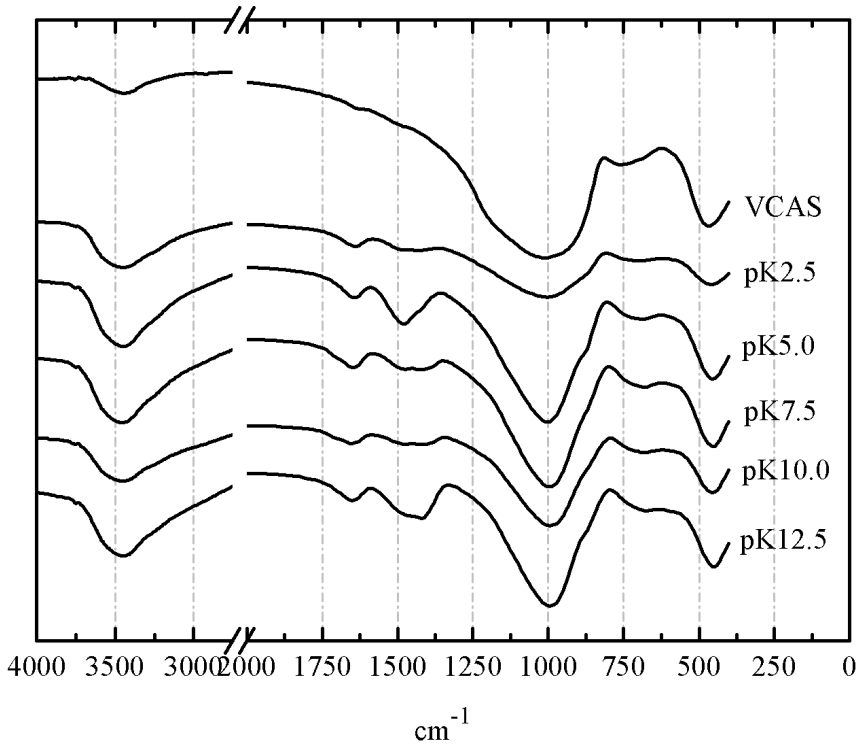

Figure 5. FTIR spectra for VCAS sample and AA-VCAS pastes activated with KOH solutions.

392

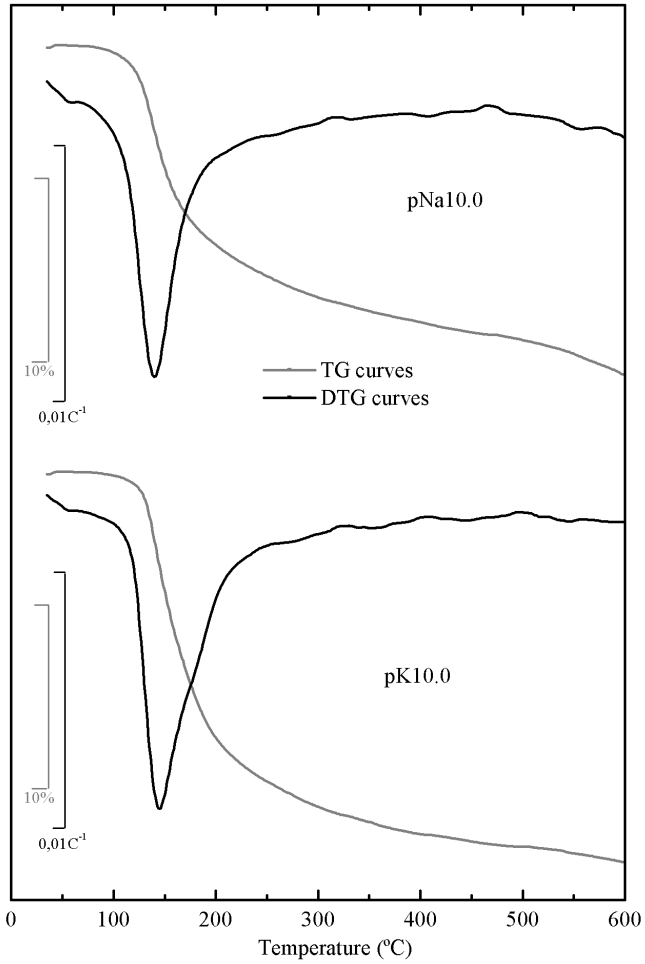

393

394 Figure 6. TG and DTG curves for alkali-activated VCAS pastes prepared using either 10

395 mol.kg^{-1} NaOH and KOH solutions.

396

397

398

399

400

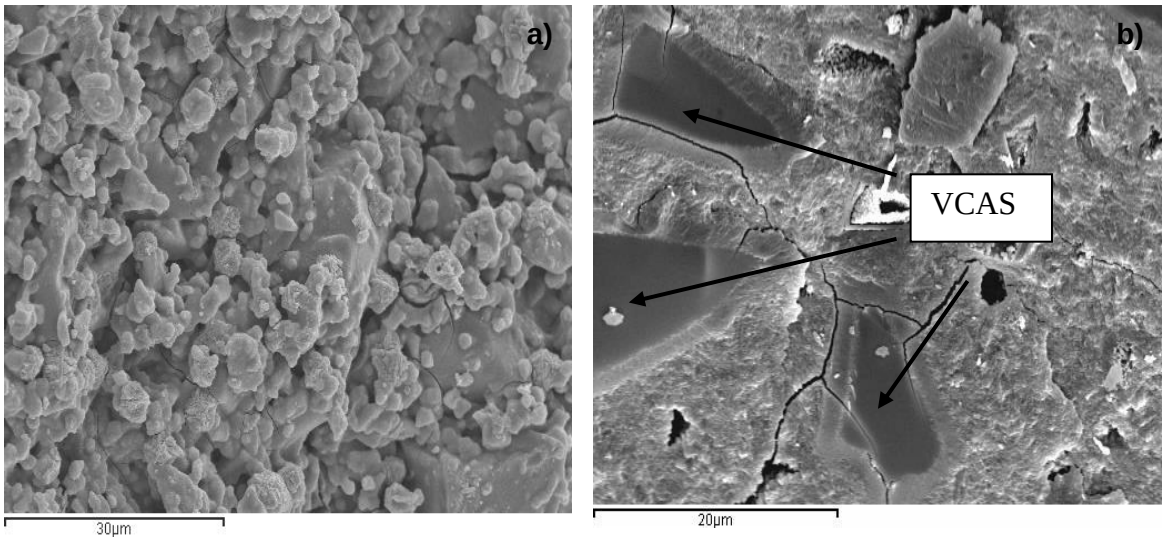

Figure 7. SEM images of pastes activated with NaOH solutions: a) pNa5.0; b) pNa10.0

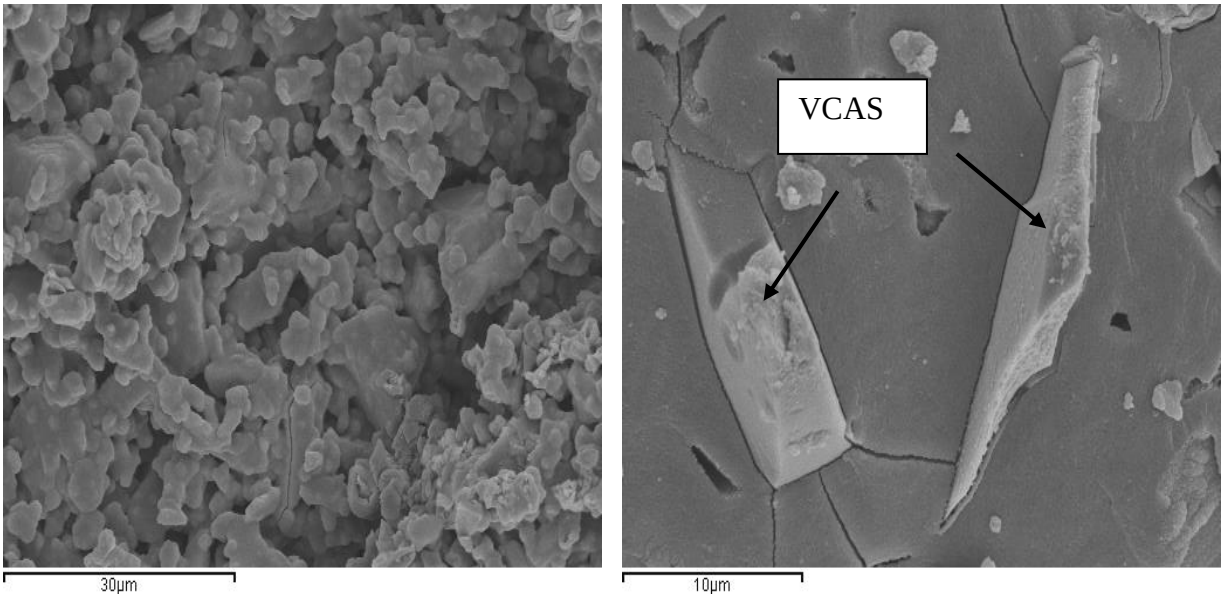

Figure 8. SEM images of pastes activated with KOH solutions: a) pK5.0; b) pK10.0

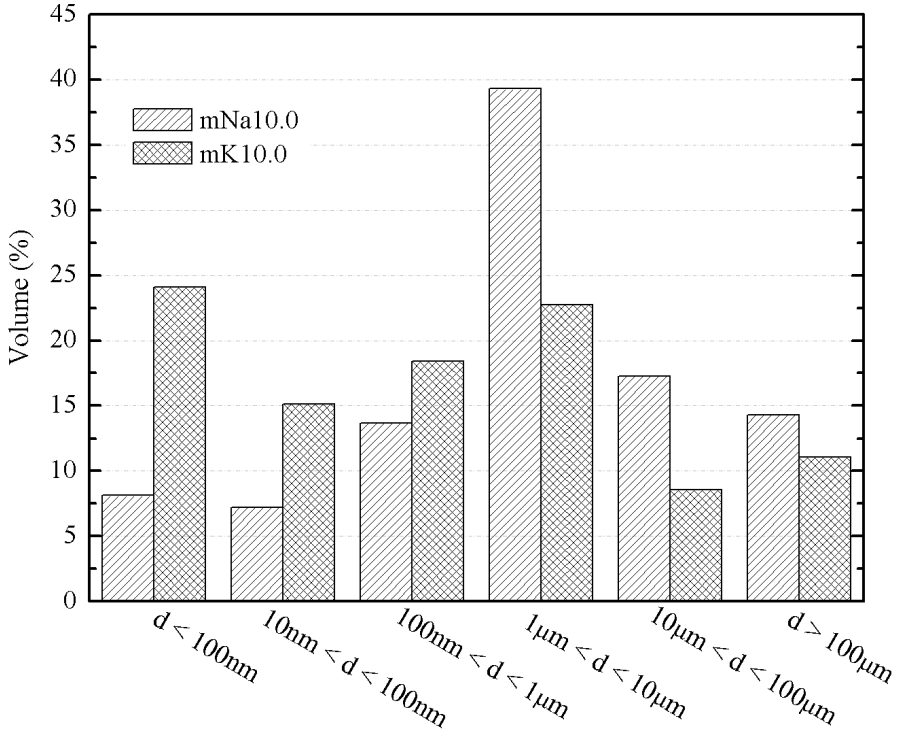

Figure 9. Pore size distribution for AA-VCAS mortars.

Table 1. Chemical composition of VCAS (% by weight).

SiO_2	Al_2O_3	CaO	MgO	Na_2O	K_2O	Fe_2O_3	Others
57.90	12.92	23.51	2.88	0.74	0.13	0.47	1.45

Table 2. Mix proportions of activating solutions.

Mixture	Alkali cation (M^+)	Molality (m)	w/VCAS
Na2.5	Na^+	2.5	0.45
Na5.0	Na^+	5.0	0.45
Na7.5	Na^+	7.5	0.45
Na10.0	Na^+	10.0	0.45
Na12.5	Na^+	12.5	0.45
K2.5	K^+	2.5	0.45
K5.0	K^+	5.0	0.45
K7.5	K^+	7.5	0.45
K10.0	K^+	10.0	0.45
K12.5	K^+	12.5	0.45

Table 3. Thermogravimetric analysis data showing the total weight loss (%) in the range 35-600ºC of alkali-activated VCAS pastes activated with NaOH and KOH solutions.

Akali concentration (C, mol.kg^{-1})	2.5	5.0	7.5	10.0	12.5
NaOH solution (pNaC)	6.95	11.09	14.24	19.17	17.78
KOH solution (pKC)	6.65	10.35	11.58	14.87	16.71

Table 4. Average compressive strengths of alkali-activated VCAS mortars cured for 3 days at 65ºC.

Alkali concentration (C, mol.kg^{-1})	2.5	5.0	7.5	10.0	12.5
NaOH solution (mNaC)	25.24 ± 2.52	49.51 ± 1.88	65.08 ± 2.50	77.18 ± 2.25	60.06 ± 2.05
KOH solution (mKC)	15.96 ± 0.76	29.88 ± 0.71	49.61 ± 0.89	70.03 ± 3.67	70.28 ± 3.10